Acta Scientiarum
http://periodicos.uem.br/ojs
ISSN on-line: 1807-8664
Doi: 10.4025/actascitechnol.v44i1.57099
CC BY

Selecting sintered capillary structure for heat pipes based on experimental thermal performance

Larissa Krambeck, Guilherme Antonio Bartmeyer, Diógenes Oliveira de Souza, Davi Fusão, Paulo Henrique Dias dos Santos and Thiago Antonini Alves*

Universidade Tecnológica Federal do Paraná, Av. Doutor Washington Subtil Chueire, 330, 84017-220, Jardim Carvalho, Ponta Grossa, Paraná, Brasil.
*Author for correspondence: E-mail: antonini@utfpr.edu.br

ABSTRACT. A selection of capillary structure of sintered copper powder for heat pipes based on the experimental thermal performance was conducted. Due to the geometric characteristics, the manufactured heat pipes can be used in electronics cooling. The heat pipes are used to enhance the heat transfer and are based on phase change. The sintered metal powder structures have a high capillary pumping, low pores, and good thermal conductivity. The heat pipes were manufactured from a straight copper pipe with an external diameter of 9.45mm, an inner diameter of 7.75mm, and a length of 200mm. The capillary structure was made of sintered copper powder with three different thicknesses (2.125mm, 1.500mm, and 0.875mm). Distilled water was used as the working fluid. Each thickness was analyzed with four different filling ratios related to the evaporator volume: 60, 80, 100, and 120%. The condenser was cooled by forced convection of air, the adiabatic section was insulated, and the evaporator was heated by an electrical resistor and was insulated from the environment with aeronautic insulation. The heat pipes were tested horizontally under different low heat loads (from 5 up to 45W). The experimental results showed that all sintered heat pipes worked satisfactorily. However, Type #3 Heat Pipe with a filling ratio of 100% showed the best thermal performance.

Keywords: Sintered powder; thickness; filling ratio; thermal performance; heat pipe; experimental.

Received on December 15, 2020.
Accepted on July 30, 2021.

Introduction

The heat pipe is a highly efficient heat transfer passive device that operates on a closed biphasic cycle and uses the latent heat of vaporization of the working fluid to transfer heat from small temperature gradients (Krambeck et al., 2021). The main advantages of a heat pipe are high thermal conductivity, no need for pumping, no moving parts, and relatively low-pressure drops (Vasiliev, 2008). The heat pipe consists of an evacuated metal tube, an internal capillary structure, and a working fluid (Krambeck, Nishida, Aguiar, Santos, & Alves, 2019). This device is applied to improve the transfer of heat in many industrial areas, such as electronics, aerospace, telecommunications, food, among others (Faghri, 2014; Nishida, Krambeck, Santos, & Alves, 2020).

The heat pipes operate according to the following principle (Groll & Rösler, 1992): in the evaporator region, heat is transferred to the heat pipe, vaporizing the working fluid contained inside this region. The steam generated is moved, due to the pressure and density differences, to the condenser where heat transported is rejected to the cold source. In the heat rejection process, the steam condenses, and the condensate returns to the evaporator closing the thermodynamic cycle. The adiabatic region may have variable dimensions or be absent and it is located between the evaporator and the condenser, being insulated from the external environment (Santos, Vicente, Reis, Marquardt, & Alves, 2017). The working fluid returns from the condenser to the evaporator due to the capillary pumping effect. A schematic diagram of the operating principle of heat pipes is presented in Figure 1 (Santos, Krambeck, Santos, & Alves, 2014). More details on the principle of the heat pipes can be found in Chi (1976), Peterson (1994), Reay, Kew, and McGlen (2014), Faghri (2016), and Mantelli (2021).

The function of the capillary structure is to promote capillary pumping and the way to flow the working fluid (Santos, Alves, Oliveira Junior, & Bazzo, 2020). Thus, it directly influences the thermal performance of a heat pipe (He et al., 2020). Capillary structures of sintered metal powders are made from the sintering process, where the powder particles melt resulting in a continuous medium of flow (Krambeck, Bartmeyer,

Fusão, Santos, & Alves, 2020). The sintering is performed by heating the casing tube with the metallic powder particles and the aid of a mandrel. In this way, the metallic powder particles sinter between them and the inner wall of the tube (Tang, Deng, Huang, Wan, & Lu, 2013). The mandrel model is made of material without chemical compatibility so that it is easily removed after the sintering is finished. Sintered capillary structures have a high capillary pumping, low pores, and good thermal conductivity (Khalili & Shafii, 2016). The main parameters that influence the sintering process are process time, temperature, particle size, and atmosphere (German, 1994).

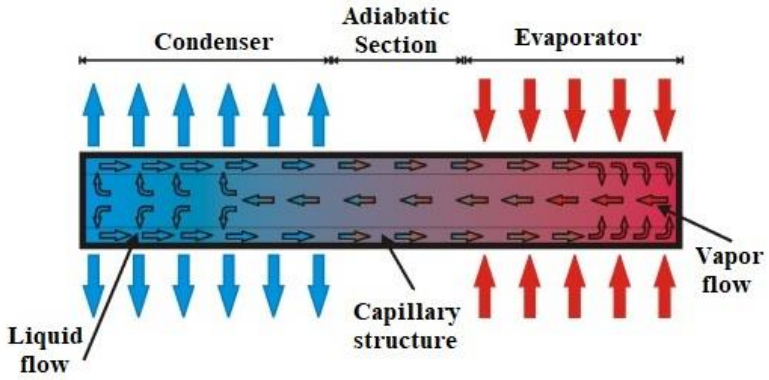

Figure 1. Sketch of the operating principle of a heat pipe.

In this research a selection of capillary structure of sintered copper powder for heat pipes based on the experimental thermal performance was conducted. Due to the geometric characteristics, the manufactured heat pipes can be used in electronics cooling (Alves & Altemani, 2008; 2011). The heat pipes were produced with spherical copper powder and temporary mandrels, which placed powder in the annulus region. The best filling ratio was determined for each type of sintered capillary structure. The analyzed operating position was horizontal.

Methodology

The methodology for manufacture (cleaning, assembly, tightness test, evacuation procedure, and filling with the working fluid); tests; and analysis of the heat pipes were developed based on Alves, Krambeck, and Santos (2018).

Characteristics of the Heat Pipes

The heat pipes were produced by straight copper tubes (ASTM B75 Alloy 122) with an outer diameter of 9.45mm, an inner diameter of 7.75mm, and a length of 200mm. The heat pipes have an evaporator region of 80mm in length, an adiabatic region of 20mm, and a condenser region of 100mm. The capillary structure was made of sintered copper powder with three different thicknesses: 2.125mm (Type #1), 1.500mm (Type #2), and 0.875mm (Type #3), as shown in Figure 2. Distilled water was used as the working fluid. Each thickness was investigated with four different filling ratios related to the evaporator volume: 60, 80, 100, and 120%. Table 1 presents the main characteristics of heat pipes analyzed in this research.

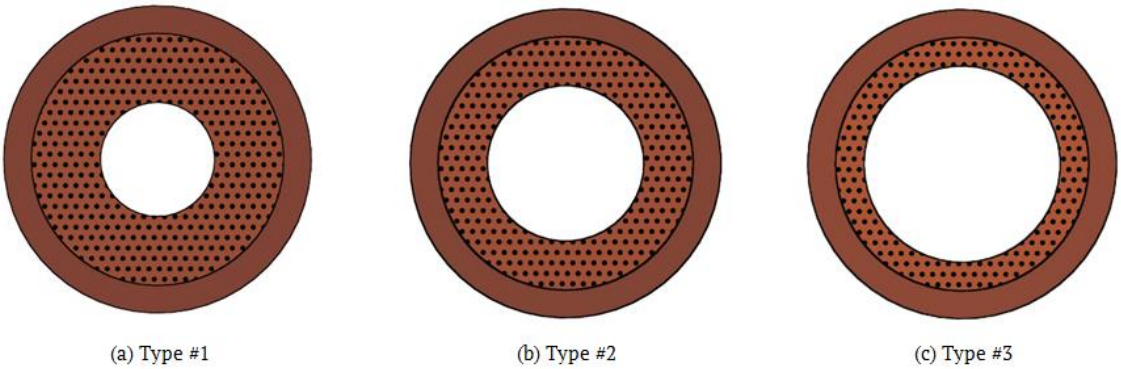

Figure 2. Configurations of capillary structures made of sintered copper powder.

Table 1. Main characteristics of heat pipes.

Characteristics	Heat Pipe											
	Type #1				Type #2				Type #3			
Inner diameter [mm]	7.75				7.75				7.75			
Outer diameter [mm]	9.45				9.45				9.45			
Evaporator [mm]	80				80				80			
Adiabatic section [mm]	20				20				20			
Condenser [mm]	100				100				100			
Capillary structure	Sintered Copper Powder											
Thickness of capillary structure [mm]	2.125				1.500				0.875			
Working fluid	Distilled water											
Filling ratio [%]	60	80	100	120	60	80	100	120	60	80	100	120
Volume of working fluid [mL]	1.54	2.06	2.57	3.09	1.70	2.27	2.83	3.40	1.90	2.54	3.17	3.80

Characteristics of the Sintered Capillary Structures

The sintered capillary structures were fabricated from a copper powder obtained by gas atomization. A photograph of the copper powder is shown in Figure 3(a). A Tescan™ VEGA3 Scanning Electron Microscopy (SEM) was used to observe the shape of the copper particles. As a result, a micrograph with a magnification of 500 times was taken. The format is approximately spherical and is presented in Figure 3(b). The chemical composition of the copper metal powder was determined by a Shimadzu™ EDX-7000 Energy Dispersive X-Ray Fluorescence Spectrometer (ED-XFR). The result showed that the metallic powder was composed of 100% copper, so the purity is very high. According to the results of the SEM and the ED-XFR, the high purity and the shape are exactly the same as expected from the powder manufacturing method (Bartmeyer, Krambeck, Silva, Fusão, & Alves, 2018).

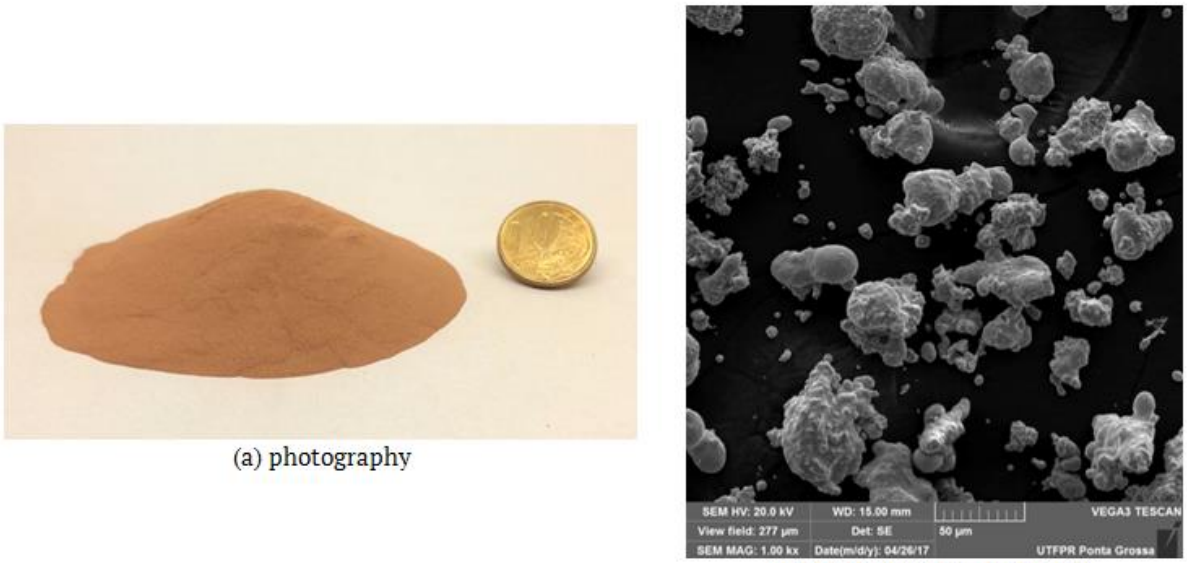

(a) photography

(b) SEM micrography (500x)

Figure 3. Copper powder used in the sintering.

For the determination of the average particle size, the Laser Diffraction Method was applied. This technique consists of the scattering of light in a sample of a powder dispersed in an aqueous medium. A Cilas™ 920 Particle Size Analyzer for a range of 0.3 and 400µm was used to measure the particle size by the Fraunhofer Diffraction Technique. In this particle size distribution analysis, alcohol was used as the dispersing agent under ultrasonic shaking for a period of 60s. Figure 4 presents this particle size distribution for copper powder. In this graph, X-axis shows the particle diameter [µm], and the Y-axis, the relative [%] and the cumulative [%] frequencies. The solid line represents the cumulative frequency for each particle size, defined with 30 size classes. The volume-based average particle diameter of the copper powder was 33µm. According to the distribution, the copper powder behavior is unimodal, which means that there is a size with more frequency. The unimodal distribution is excellent for application as the capillary structure of heat pipes (Bartmeyer et al., 2018).

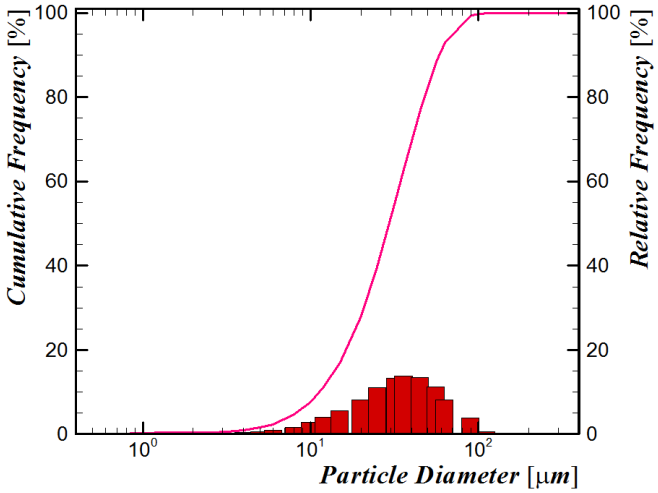

Figure 4. Particle size distribution of the copper powder.

The copper powder was sintered in straight copper tubes ASTM B-75 Alloy 122 with an outer diameter of 9.45mm, an inner diameter of 7.75mm, and a length of 250mm. AISI 304 stainless steel bar chucks with different diameters and, to maintain concentricity, SAE 1020 carbon steel supports assisted the capillary structure fabrication. Figure 5 presents the sintering process with the unimodal copper powder, the temporary mandrel, and the supports that produced the sintered heat pipes.

Figure 5. Preparation of the heat pipe for sintering process.

The apparatus used in the sintering process consisted of a controlled atmosphere horizontal tubular furnace (Inti™ FT-1200), a data acquisition system (Agilent™ 34970A with 20 channels), and a laptop (Dell™) – Figure 6. The gas used in the atmosphere control was a mixture of 95% of Argon and 5% of Hydrogen. For the evaluation of the temperature inside the furnace, a K-type thermocouple Omega Engineering™ was used.

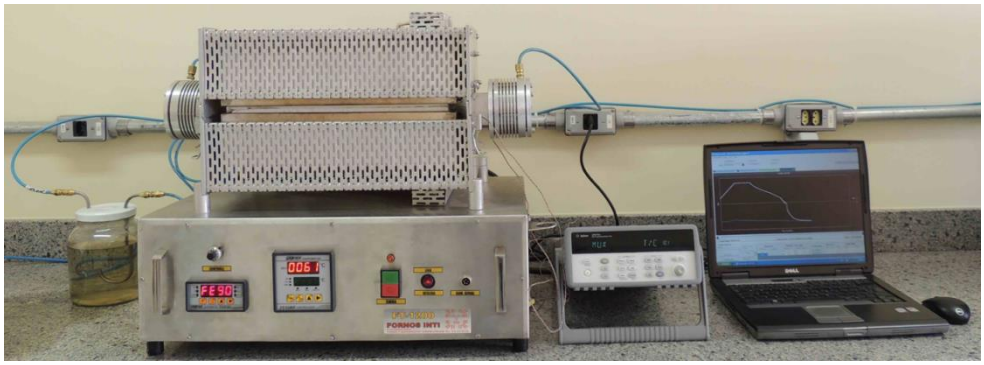

Figure 6. Experimental apparatus for the sintering process.

The sintering occurred at a heating rate of 20°C min^{-1}, with 15-minute permanency at a temperature of 800°C, and subsequent cooling by forced convection of air. Thus, the sintering process was carried out until the initial stage, which characterizes the sintering process as incomplete (Krambeck et al., 2019). The thermal curve obtained in the sintering procedure used in this study is shown in Figure 7.

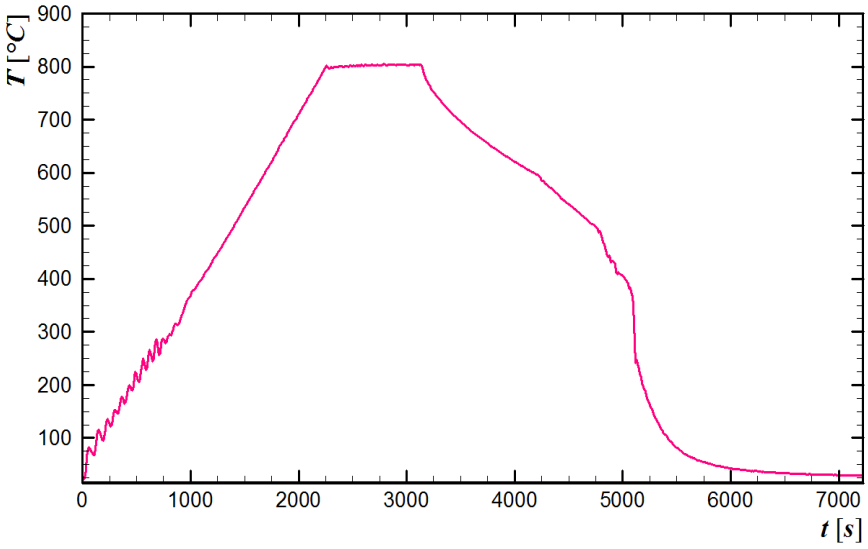

Figure 7. Sintering curve of the capillary structures.

Figure 8 shows a sample of each type of capillary structure, with different thicknesses, obtained through the sintering process. The micrograph of the sintered capillary structure is presented in Figure 9. The image was from Backscattered Electron Detector (BSD) for Scanning Electron Microscope (SEM).

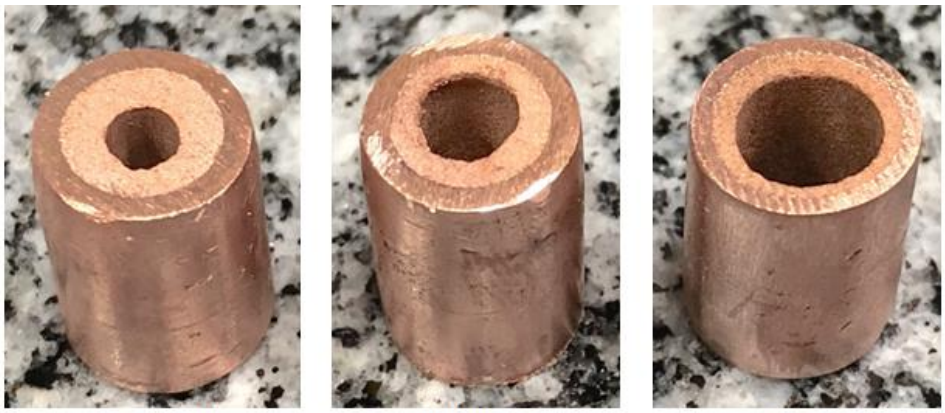

Figure 8. Sample of the sintered capillary structure configurations.

The wick porosity was obtained by Quantachrome Instruments™ Ultrapycnometer 1000 Helium Pycnometry associated with physical characterization by the Archimedes method showing that the total porosity of the capillary structure was 54.79%. For this, three samples were manufactured, by the same process and sintering parameters of the heat pipes, with a diameter and height of 20 mm. Additional characteristics of the sintered heat pipe are in Krambeck et al. (2020).

A Capillary Extrusion Test performed the determination of the capillary structure permeability, based on the MPIF Standard 39 (Metal Powder Industries Federation [MPIF], 1997). Three samples were made with a diameter of 28.7mm and a height of 3.2mm. The sintering procedure was the same as applied to the capillary structure of sintered copper powder of the heat pipes. The average permeability of the capillary structure of copper powder was 7.81 x 10^{-13} ± 0.38 x $10^{-13}$$m^2$. The experimental results were compared to the models proposed in the literature by Kaviany (1995). The results were compared considering the distribution of the particle size, with the diameters corresponding to each quartile of the particle size distribution (11.3μm,

29.5µm, and 58.3µm) and the average particle diameter of 33µm. Moreover, the theoretical analysis considered the experimental porosity of the structure of 55.03%, obtained by Krambeck, Bartmeyer, Fusão, Santos, and Alves (2019). The experimental results show a better match with the theoretical models for smaller particle diameters (the particle size of the first quartile).

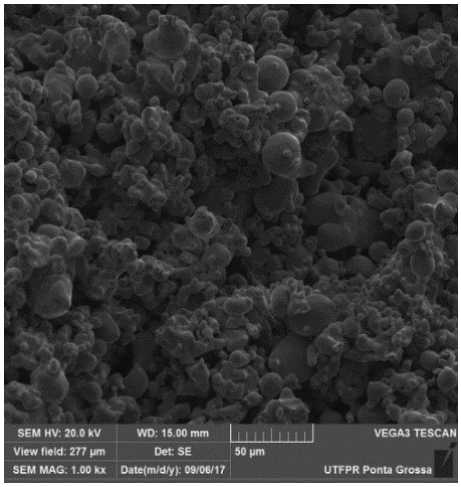

Figure 9. Micrograph of the sintered capillary structure (500x).

The critical radius of the capillary structure was measured by the MPIF Standard 39 (MPIF, 1997), with the same experimental bench that was used for permeability determination. The average critical radius measured experimentally was 6.57µm. The theoretical critical radius is 6.765µm (Florez, Mantelli, & Nuernberg, 2013). Considering the experimental uncertainty, the results of the samples are similar and in agreement with the literature.

An experimental workbench based on the guarded-hot-plate principle, an adaptation of ABNT NBR 15220 - Part 04 (Associação Brasileira de Normas Técnicas [ABNT], 2003), was developed to evaluate the effective thermal conductivity of the sintered wick. Three samples were sintered with a squared face of 37.5mm and an area of 1,406.25mm^2. The difference between the samples was the thickness, which was 13.0mm, 8.4mm, and 5.0mm for samples A, B, and C, respectively. The sintering procedure was the same that was applied to the heat pipes subsequently. The average effective thermal conductivity of the capillary structure was 15.13W mK^{-1}. The theoretical model (Atabaki & Baliga, 2007) resulted in thermal conductivity of 15.55W mK^{-1}, since the average porosity of this sintered structure was 55.03%. As a result, the experimental value of the effective thermal conductivity is close to the theoretical value. The difference is 2.89% that validates the proposed experimental apparatus to determine the effective thermal conductivity.

Experimental apparatus of thermal tests

The experimental apparatus used for the experimental tests, shown in Figure 10, is composed of a power supply unit (Agilent™ U8002A), a data logger (Agilent™ 34970A with 20 channels), a laptop (Dell™), an uninterruptible power supply (NHS™), a universal support, and a fan (Ultrar™).

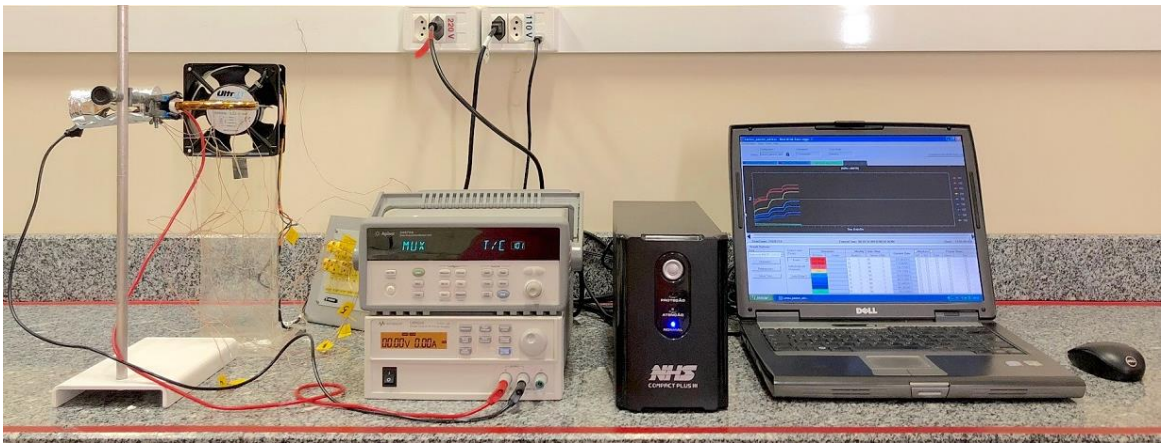

Figure 10. Experimental apparatus for thermal tests.

For the evaluation of the thermal performance of the heat pipes, K-type thermocouples Omega Engineering™ were used. They were fixed on the outer surface of the heat pipe by a thermosensitive adhesive strip Kapton™. As shown in Figure 11, there were three thermocouples in the evaporator ($T_{evap,1}$, $T_{evap,2}$, and $T_{evap,3}$), one thermocouple in the adiabatic section (T_{adiab}) e four thermocouples in the condenser ($T_{cond,1}$, $T_{cond,2}$, $T_{cond,3}$, and $T_{cond,4}$) in heat pipes.

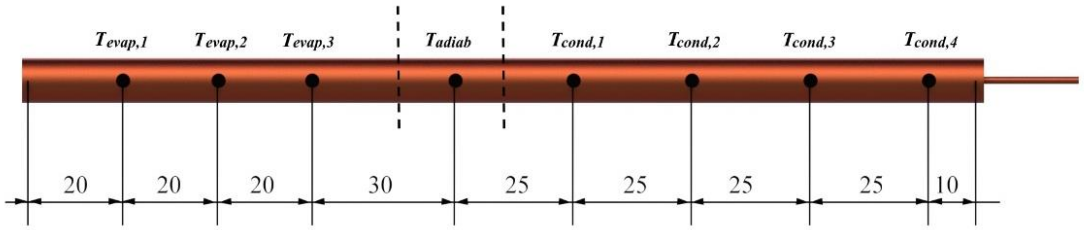

Figure 11. Thermocouple positions [mm].

The heating system of the evaporator is conducted by power dissipation from the passage of an electric current in a nickel-chromium alloy power strip resistor Omega Engineering™ with 0.1mm of thickness and 3.5mm of width. To ensure that the generated heat by the Joule effect is transmitted to the evaporator, an aeronautic thermal insulation MTI Polyfab™ and a layer of polyethylene 3M™ are installed in this region. A fiberglass tape Omega Engineering™ is used in the adiabatic section as heat insulation between the support and the heat pipe. The cooling system using forced convection of air consisted of a fan in the condenser region. Details of the heat pipe regions are shown in Figure 12.

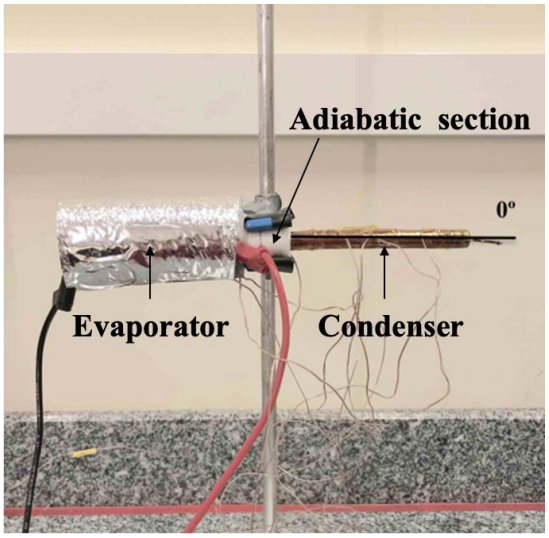

Figure 12. Heat pipe regions.

Experimental Procedure

To ensure the best results and the repeatability of experimental tests, the ambient temperature was maintained at 20°C ± 1°C. A thermal conditioning system Carrier™ was used for this purpose. A detailed check of the equipment and the heat pipe (fixing thermocouples, thermal insulation, resistor connection, among others) must be performed before each experimental test. The heat pipe was carefully fixed to the universal support bracket in the adiabatic region in the desired position. The cooling system was set at a speed of 5m s^{-1} controlled by a potentiometer with a combined error of ± 0.2m s^{-1}. The average air velocity was calculated following the ASHRAE Handbook (American Society of Heating, Refrigerating and Air-Conditioning Engineers [ASHARE], 2017). The data acquisition system was turned on, collecting the temperatures measured by the K-type thermocouples. The temperatures should be verified according to the ambient temperature, and if these were stable and approximately 20°C, finally, the heating system can be turned on and adjusted to the dissipation power desired. The initial load was 5W and, after about 15 minutes, the thermocouples showed stationary values. If it happened, the thermal load has been

increased by 5W. The load increment was made until the maximum temperature of the device reached the critical temperature (160°C), where the melting of the materials could happen. Data were acquired every 5s, recorded on the laptop by the software Agilent™ Benchlink Data Logger 3.

Data Reduction

The thermal performance of the heat pipes was analyzed and compared by the operating temperature (T_{op}) and the global thermal resistance (R_{th}). The analyzed operating temperature is the temperature of the adiabatic region. The global thermal resistance, R_{th}, of a heat pipe can be defined as the ratio between the total temperature drop across the device and the total heat transfer (Rohsenow, Hartnett, & Cho, 1998). The higher the thermal resistance, the greater the difficulty of transporting heat from the system (Bergman, Lavine, Incropera, & DeWitt, 2017). The total thermal resistance can be calculated by

$$R_{th} = \frac{\Delta T}{q} = \frac{\left(T_{evap} - T_{cond}\right)}{q}, \quad (1)$$

where, q is the heat transfer capability of the device [W], T_{evap} and T_{cond} are the mean temperature of the evaporator and the condenser, respectively [ºC].

The measurement uncertainties were estimated for the temperature and heat load. Considering the accuracy of the temperature sensors (K-type thermocouples) and the data logger, the temperature uncertainty was estimated at ± 1.27ºC. The uncertainty of the electrical power input was valued at ± 1%, including the uncertainty of the power supply unit and the data logger. The uncertainties are shown in the obtained results. For the correlated uncertainties determination, the error propagation method described by Holman (2011) was used.

Results and discussion

The experimental results regarding the thermal performance of the heat pipes with different sintered capillary structures are presented. According to the proposed experimental procedure, the temperature distribution verified during the experimental tests for each thermocouple tends to the same aspect, modifying only the magnitude of the values. These values are treated and evaluated later according to the operating temperature and thermal resistance, allowing a better comparison between the heat pipes. The thermal results involve the filling ratio and thickness comparisons.

The tests were performed at increasing heat loads of 5W, ranging from 5 to 45W for the horizontal position. Figure 13 illustrates the temperature distributions as a function of time for the three types of heat pipe. Due to many results, only the best filling ratio of each configuration is shown in Figure 13.

The evaporators of the heat pipes obtained an isothermal behavior, while the condensers showed a gradient between the temperatures of the four thermocouples in the region. The reason for that is an irregular flow in the condenser region in the azimuth direction (Souza et al., 2021). With each increase in heat load, the temperatures of the heat pipes also rise. The steam front is advancing from the evaporator to the condenser as the temperatures along the heat pipes approach the evaporator temperatures. As a result, every heat pipe operated satisfactorily. Type #2 and Type #3 reached a quasi-permanent regime around 300s after the first thermal load, while Type #2 achieved this condition in the second heat load. For the 45W thermal load, the pre-established critical temperature for the evaporator average (160°C) was reached in Type #1 and Type #2, and the test ended. However, Type #3 reached the critical temperature limit at 50W.

Filling ratio analysis

The experimental results of the filling ratios related to the evaporator volume of 60, 80, 100, and 120% for Type #1, Type #2, and Type #3 are taken, concerning their operating temperatures and thermal resistances. Figure 14 shows the behavior of the operating temperature in the quasi-permanent regime of the three configurations, with different filling ratios, for the heat loads dissipated horizontally. The combined uncertainty of the operating temperature is 1.27°C.

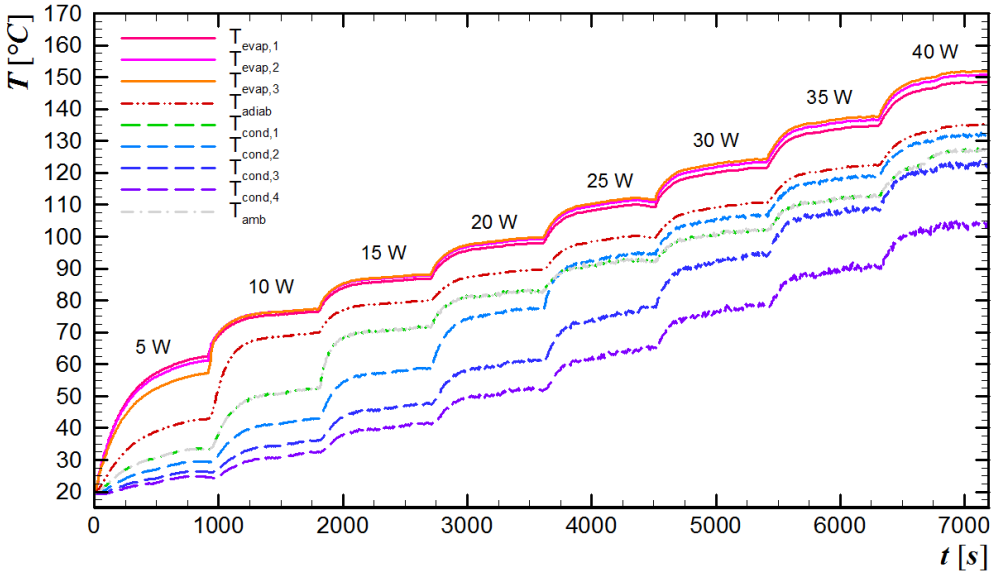

(a) Type #1

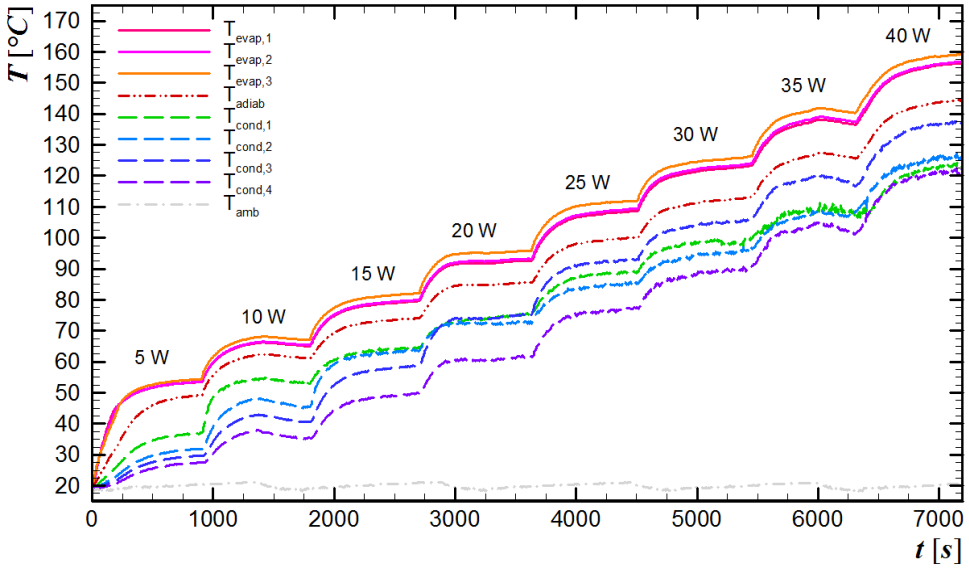

(b) Type #2

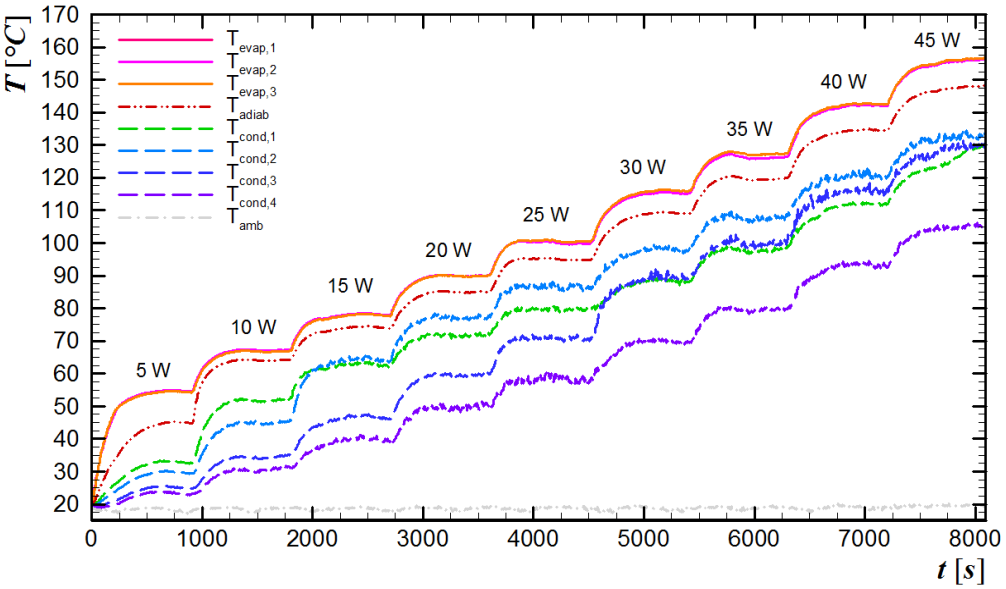

(c) Type #3

Figure 13. Temperature distribution *versus* time of the heat pipes.

In all the presented cases, the trend was to increase the operating temperature with the rise in the dissipated power as expected. For Type #1, Figure 14(a), the heat pipe with a filling ratio of 120% was the one that holds out higher powers; however, its operating temperature behavior was not linearly corresponding to the increase in dissipation. The other filling ratios showed a linear behavior. The heat pipe of Type #2, the heat pipe temperatures of 80 and 100% were very close and the lowest - Figure 14(b). The linear behavior of the temperatures with the increase in power was not observed just for the tube with a 60% filling ratio. In Type #3 cases, Figure 14(c), the operating temperatures of the heat pipes with different filling ratios were very close to the horizontal one. The heat pipe with 100% filling ratio was the one that withstood a greater power.

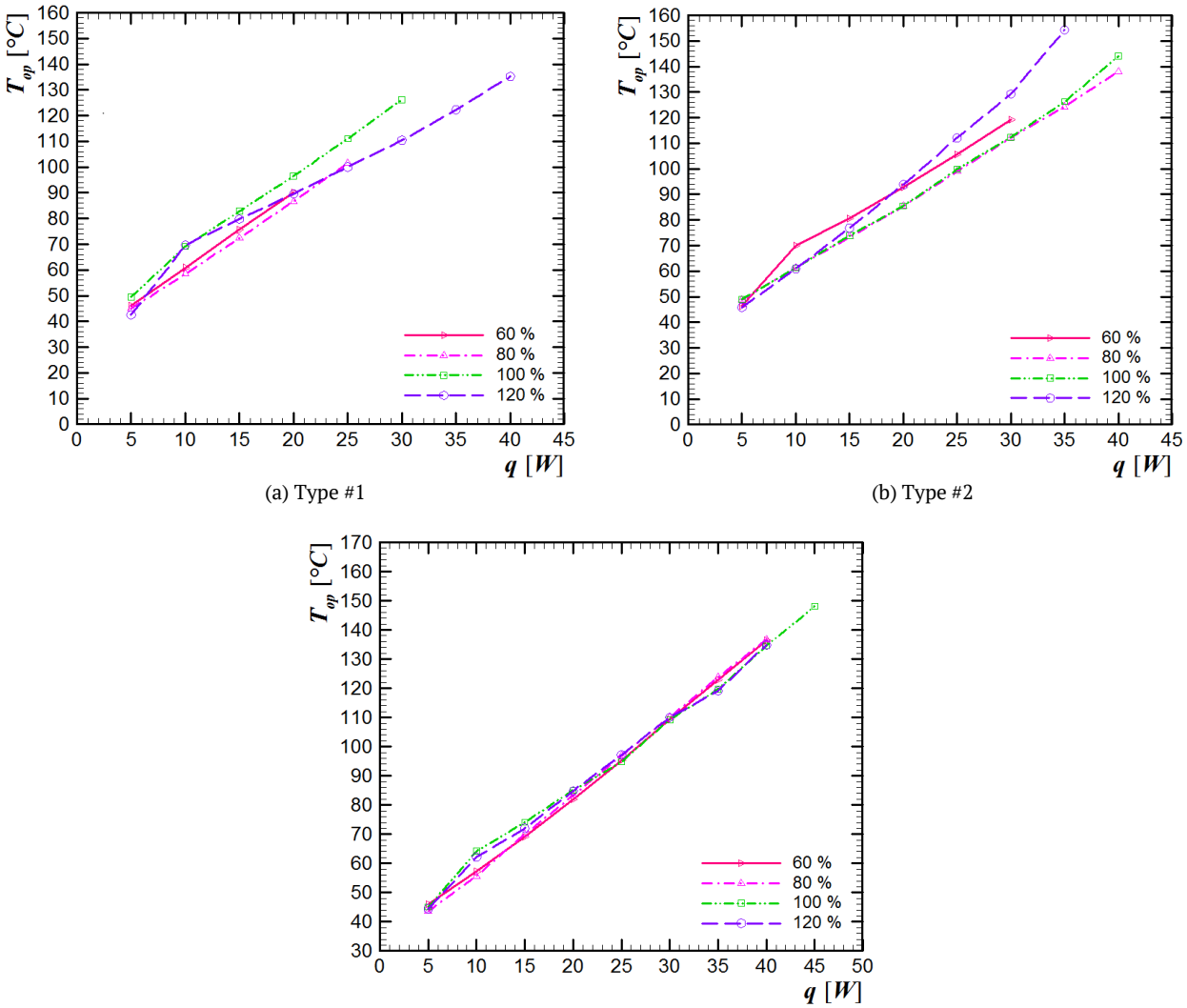

(a) Type #1

(b) Type #2

(c) Type #3

Figure 14. Operating temperature for different filling ratios of each capillary structure.

Figure 15 presents the global thermal resistance for three types of the capillary structure as a function of the power dissipated horizontally. The vertical bars indicate the experimental uncertainties of the measurements. As expected, the thermal resistances of the sintered heat pipes decreased with the increase in the dissipated power, working satisfactorily.

The heat pipe with the largest thickness of sintered powder, Type #1, which had the lowest thermal resistance and withstand the highest heat load, 40W, that is, with the best thermal performance from 25W, was the one with the filling ratio of 120% of the evaporator volume. The heat pipe with 60% filling ratio showed the highest thermal resistance and the worst thermal behavior due to the lack of working fluid in the evaporator. Heat pipes with 80 and 100% filling ratios, on the other hand, presented satisfactory thermal performances, but for applications with high power, 40W, their operating temperatures would be too high, which could make their use unfeasible. For Type #2, the thermal resistance of 60% was the highest due to the probable drying of the evaporator's working fluid. The 80, 100, and 120% filling ratios showed thermal

resistance with very similar behavior. Due to a lower resistance, the heat pipe with 100% filling ratio presented the best thermal performance. According to Figure 15(c), in cases Type #3, despite not having a lower thermal resistance, the heat pipe with a filling ratio of 100% would be the most suitable due to the ability to withstand a greater power, 45W.

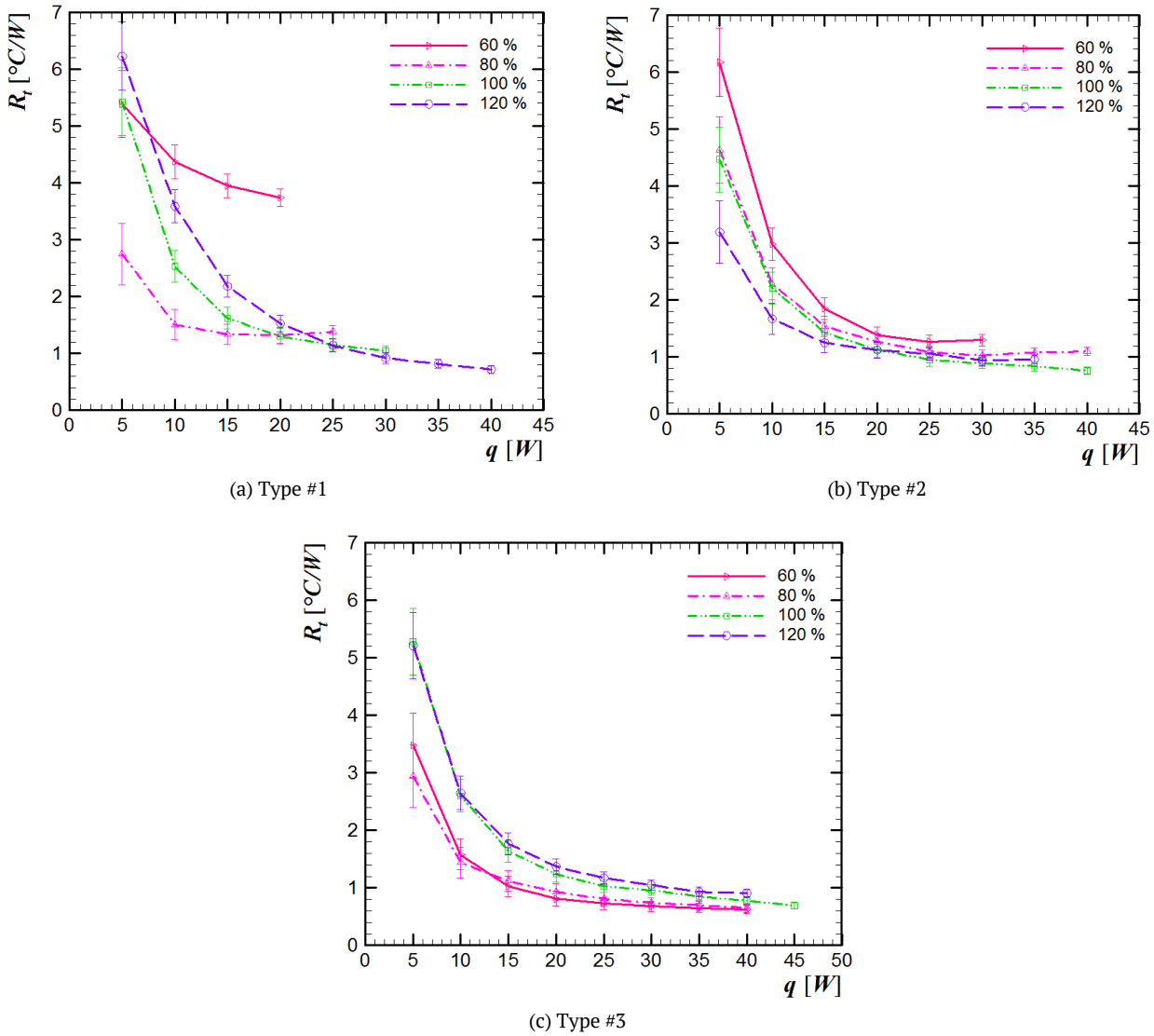

(a) Type #1

(b) Type #2

(c) Type #3

Figure 15. Thermal resistance for different filling ratios of each capillary structure.

The best filling ratio gives the lowest operating temperature, a higher power dissipation, and values of lower thermal resistance. Thus, for Type #1, the best filling ratio was 120% of the evaporator volume. Although the operating temperature of Type #2 with 100% evaporator filling ratio was not the lowest, its thermal resistance was the lowest, especially for high dissipated powers. Thus, the best filling ratio for Type #2 was 100%. As for Type #2, the best filling ratio was 100% for Type #3.

Thickness Influence

Knowing the best performance of each type of heat pipe, the comparison of capillary structures of sintered powder can be performed. The behavior of the operating temperature as a function of the dissipated power for different sintered heat pipes is compared in Figure 16. As the thermal load increases, the operating temperature also increases for all types of sintered heat pipes. By comparing the best filling ratios of each configuration, it is possible to verify that the performances of the heat pipes are very similar. In general, the operating temperatures ranged from 40 to 145°C. Besides, all types supported the power of at least 40W. Thus, according to the operating temperature for thermal loads of up to 40W, we could use any heat pipe configuration. However, if the application requires a power dissipation of 45W, Type #3 would be the most appropriate.

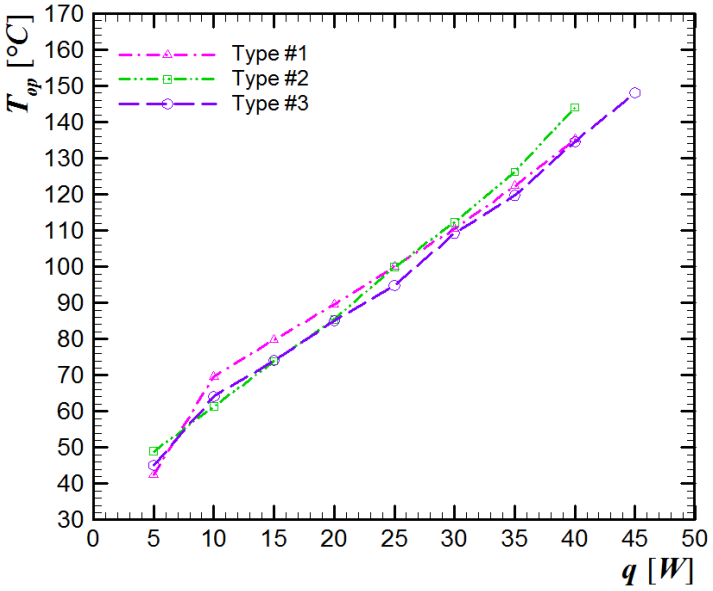

Figure 16. Operating Temperature *versus* power dissipation.

Figure 17 presents the global thermal resistance as a function of the power dissipation considering the three thicknesses of the sintered capillary structure. As the heat dissipation grows, the thermal resistance decreases for the heat pipes in the horizontal position. The thermal resistances are very similar and present satisfactory performances. Thermal resistances range from 6.5 to 0.5°C W^{-1}.

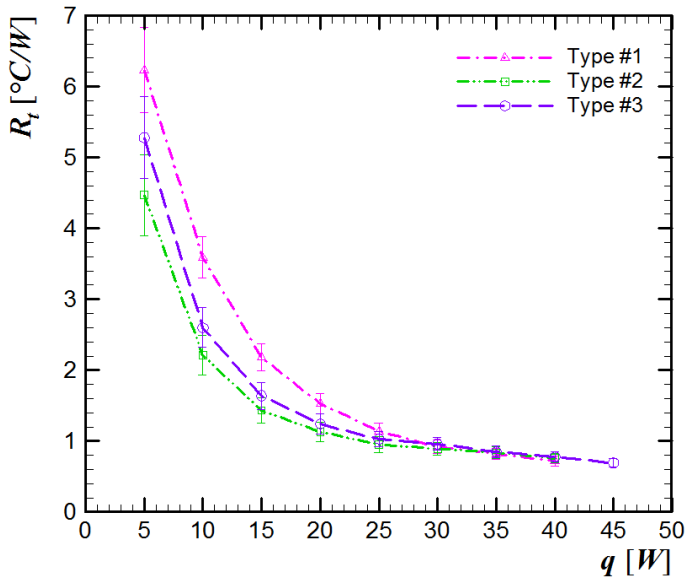

Figure 17. Thermal resistance *versus* power dissipation.

The experimental results showed that all sintered heat pipes worked satisfactorily; however, the sintered capillary structure with a thickness of 0.875mm, Type #3, with a filling ratio of 100% showed the best thermal performance because it can withstand a higher power dissipation.

Conclusion

In this research a selection of capillary structure of sintered copper powder for heat pipes based on the experimental thermal performance was conducted. Due to the geometric characteristics, the manufactured heat pipes can be used in electronics cooling. A sintered copper powder composed the wicks with thicknesses of 2.125, 1.500, and 0.875mm. The heat pipes were tested horizontally under different low heat loads (from 5 up to 45W). Distilled water was the working fluid, and the best filling ratio was determined for each type of capillary structure. As a result of the study, all the sintered heat pipes worked successfully and as expected.

Due to lower operating temperature, a higher power dissipation, and values of lower thermal resistance, the best filling ratio for the Type #1, Type #2, and Type #3 was 120, 100, and 100% of the evaporator volume, respectively. The sintered capillary structure with a thickness of 0.875mm, Type #3, showed the best thermal performance.

Acknowledgements

Acknowledgments are provided to the Capes (Coordenação de Aperfeiçoamento de Pessoal de Nível Superior), the CNPq (Conselho Nacional de Desenvolvimento Científico e Tecnológico), the PROPPG/UTFPR (Pró-Reitoria de Pesquisa e Pós-Graduação), the DIRPPG/UTFPR (Diretoria de Pesquisa e Pós-Graduação), the PPGEM/UTFPR/ Campus Ponta Grossa (Programa de Pós-Graduação em Engenharia Mecânica), and the DAMEC/UTFPR/Campus Ponta Grossa (Departamento Acadêmico de Mecânica).

References

Alves, T. A., & Altemani, C. A. C. (2008). Convective cooling of three discrete heat sources in channel flow. *Journal of the Brazilian Society of Mechanical Sciences and Engineering, 30*(3), 245-252. DOI: https://doi.org/10.1590/S1678-58782008000300010

Alves, T. A., & Altemani, C. A. C. (2011). Conjugate cooling of a discrete heat in laminar channel flow. *Journal of the Brazilian Society of Mechanical Sciences and Engineering, 33*(3), 278-286. DOI: https://doi.org/10.1590/S1678-58782011000300003

Alves, T. A., Krambeck, L., & Santos, P. H. D. d. (2018). Heat pipe and thermosyphon for thermal management of thermoelectric cooling. In P. Aranguren (Ed.), *Bringing thermoelectricity into reality* (Chapter 17, p. 353-373). London, UK: IntechOpen. DOI: https://doi.org/10.5772/intechopen.76289

American Society of Heating, Refrigerating and Air-Conditioning Engineers. [ASHARE]. (2017). *ASHARE handbook: fundamentals*. New York, NY: Ashare.

Associação Brasileira de Normas Técnicas [ABNT]. (2003). *NBR 15220: Desempenho térmico de edificações. Parte 1: Definições, símbolos e unidades*. Rio de Janeiro, RJ: ABNT.

Atabaki, N., & Baliga, B. R. (2007). Effective thermal conductivity of water-saturated sintered powder-metal plates. *Heat and Mass Transfer, 44*(1), 85-99. DOI: http://doi.org/10.1007/s00231-007-0229-8

Bartmeyer, G. A., Krambeck, L., Silva, R. C. d., Fusão, D., & Alves, T. A. (2018). Characterization of a copper powder for heat pipe wick applications. *International Journal of Advanced Engineering Research and Science, 5*(10), 52-54. DOI: http://doi.org/10.22161/ijaers.5.10.7

Bergman, T. L., Lavine, A. S., Incropera, F. P., & DeWitt, D. P. (2017). *Fundamentals of heat and mass transfer*. New Jersey, NJ: John Wiley & Sons.

Chi, S. W. (1976). *Heat pipe theory and practice: a sourcebook*. Washington, D.C.: Hemisphere.

Faghri, A. (2014). Heat pipes: review, opportunities and challenges. *Frontiers in Heat Pipes, 5*, 1-48. DOI: http://doi.org/10.5098/fhp.5.1

Faghri, A. (2016). *Heat pipe science and technology*. Kanpur, IN: Global Digital Press.

Florez, J. P. M., Mantelli, M. B. H., & Nuernberg, G. G. V. (2013). Effective thermal conductivity of sintered porous media: Model an experimental validation. *International Journal of Heat and Mass Transfer, 66*(11), 868-878. DOI: https://doi.org/10.1016/j.ijheatmasstransfer.2013.07.088

German, R. M. (1994). *Powder metallurgy science*. New Jersey, NJ: Metal Powder Industry.

Groll, M., & Rösler, S. (1992). Operation principles and performance of heat pipes and closed two-phase thermosyphons. *Journal of Non-Equilibrium Thermodynamics, 17*(2), 91-151. DOI: http://doi.org/10.1515/jnet.1992.17.2.91

He, S., Zhou, P., Ma, Z., Deng, W., Zhang, H., Chi, Z., ... Liu, Z. (2020). Experimental study on transient performance of the loop heat pipe with a pouring porous wick. *Applied Thermal Engineering, 164*, 114450. DOI: http://doi.org/10.1016/j.applthermaleng.2019.114450

Holman, J. (2011). *Experimental methods for engineers*. New York, NY: McGraw-Hill.

Kaviany, M. (1995). *Principles of heat transfer in porous media*. New York, NY: Springer Verlag.

Khalili, M., & Shafii, M. B. (2016). Experimental and numerical investigation of the thermal performance of

a novel sintered-wick heat pipe. *Applied Thermal Engineering, 94*, 59-75. DOI: http://doi.org/10.1016/j.applthermaleng.2015.10.120

Krambeck, L., Bartmeyer, G. A., Fusão, D., Santos, P. H. D. d., & Alves, T. A. (2019). Permeability of a capillary structure of sintered copper powder used in heat pipes. *International Journal of Advanced Engineering Research and Science, 6*(2), 199-202. DOI: http://doi.org/10.22161/ijaers.6.2.26

Krambeck, L., Bartmeyer, G. A., Fusão, D., Santos, P. H. D., & Alves, T. A. (2020). Experimental research of capillary structure technologies for heat pipes. *Acta Scientiarum. Technology, 42*(1), e48189. DOI: http://doi.org/10.4025/actascitechnol.v42i1.48189

Krambeck, L., Bartmeyer, G. A., Souza, D. O., Fusão, D., Santos, P. H. D., & Alves, T. A. (2021). Experimental thermal performance of different capillary structures for heat pipes. Energy Engineering: *Journal of the Association of Energy Engineers, 118*(1), 1-14. DOI: http://doi.org/10.32604/EE.2020.013572

Krambeck, L., Nishida, F. B., Aguiar, V. M. d., Santos, P. H. D. d., & Alves, T. A. (2019). Thermal performance evaluation of different passive devices for electronics cooling. *Thermal Science, 23*(2), 1151-1160. DOI: http://doi.org/10.2298/TSCI170610300K

Mantelli, M. B. H. (2021). *Thermosyphons and heat pipes: theory and applications*. Cham, SW: Springer Nature.

Metal Powder Industries Federation [MPIF]. (1997). *MPIF Standard 39: Determination of properties of sintered bronze PM filter powders*. New Jersey, NJ: MPIF.

Nishida, F. B., Krambeck, L., Santos, P. H. D. d., & Alves, T. A. (2020). Experimental investigation of heat pipe thermal performance with microgrooves fabricated by wire electrical discharge machining (wire-EDM). *Thermal Science, 24*(2), 701-711. DOI: http://doi.org/10.2298/TSCI180227206B

Peterson, G. P. (1994). *An introduction to heat pipes: modeling, testing, and applications*. Toronto, CA: John Wiley & Sons.

Reay, D., Kew, P., & McGlen, R. (2014). *Heat pipes: theory, design and applications*. Amsterdam, NL: Butterworth-Heinemann.

Rohsenow, W. M., Hartnett, J. P., & Cho, Y. I. (1998). *Handbook of heat transfer*. New York, NY: McGraw-Hill.

Santos, P. H. D., Alves, T. A., Oliveira Junior, A. A. M., & Bazzo, E. (2020). Analysis of a flat capillary evaporator with a bi-layered porous wick. *Thermal Science, 24*(3B), 1951-1962. DOI: https://doi.org/10.2298/TSCI180419240S

Santos, P. H. D. d., Krambeck, L., Santos, D. L. F. d., & Alves, T. A. (2014). Analysis of a stainless steel heat pipe based on operation limits. *International Review of Mechanical Engineering – IREME, 8*(3), 599-608. DOI: http://doi.org/10.15866/ireme.v8i3.902

Santos, P. H. D. d., Vicente, K. A. T., Reis, L. d. S., Marquardt, L. d. S., & Alves, T. A. (2017). Modeling and experimental tests of a copper thermosyphon. *Acta Scientiarum. Technology, 39*(1), 59-68. DOI: http://doi.org/10.4025/actascitechnol.v39i1.28957

Souza, D. O. d., Machado, P. L. O., Chiarello, C., Santos, E. N. d., Silva, M. J. d., Santos, P. H. D. d., & Alves, T. A. (2021). Experimental study of hydrodynamic parameters regarding on geyser boiling phenomenon in glass thermosyphon using wire-mesh sensor. *Thermal Science, OnLine-First Issue*(00), 221-221. DOI: https://doi.org/10.2298/TSCI201008221O

Tang, Y., Deng, D., Huang, G., Wan, Z., & Lu, L. (2013). Effect of fabrication parameters on capillary performance of composite wicks for two-phase heat transfer devices. *Energy Conversion and Management, 66*, 66-76. DOI: http://doi.org/10.1016/j.enconman.2012.09.027

Vasiliev, L. L. (2008). Micro and miniature heat pipes - electronic component coolers. *Applied Thermal Engineering, 28*(4), 266-273. DOI: http://doi.org/10.1016/j.applthermaleng.2006.02.023